

## Impacts of Renal Denervation and Vagus Nerve Stimulation on Acute Renal Failure Induced by Renal Ischemia Reperfusion injury in Rat Model

Mohamed H ElSayed<sup>1\*</sup>, Zainab Eltayeb<sup>2</sup>, Ahmed M Abdellah<sup>3</sup>, Wessam E Morsy<sup>4</sup>, Ghusoon A Bashady<sup>5</sup>, Nada A Ebrahim<sup>5</sup> and Karim M Ellabany<sup>5</sup>

<sup>1,4</sup>Department of physiology, Faculty of medicine Ain Shams University, Egypt

<sup>2</sup>Department of Histology, Faculty of medicine, Helwan University, Egypt

<sup>3,5</sup>Animal Research and Experimental Surgery Unit of Medical Research Center, Ain Shams University, Egypt

\***Corresponding author:** Dr. Mohamed H ElSayed (MD), Assistant Professor of Physiology, Faculty of Medicine, Ain Shams University, Egypt, E-mail: doctorpioneer@yahoo.com

**Received Date:** Sep 1, 2019; **Accepted Date:** Sep 10, 2019; **Published Date:** Sep 20, 2019

**Copyright:** © 2019 El Sayed MH, et al. This is an open-access article distributed under the terms of the Creative Commons Attribution License, which permits unrestricted use, distribution, and reproduction in any medium, provided the original author and source are credited.

**Citation:** El Sayed MH, Eltayeb Z, Abdellah AM, Morsy WE, Bashady GA, et al. (2019) Impacts of Renal Denervation and Vagus Nerve Stimulation on Acute Renal Failure Induced by Renal Ischemia Reperfusion injury in Rat Model. Eur Exp Biol Vol.9 No.3:7.

### Abstract

Ischemia-Reperfusion Injury (IRI) is characterized by temporary cessation followed by restoration of blood supply and re-oxygenation of a certain organ. In the kidney, IRI contributes to Acute Kidney Injury (AKI) with rapid kidney damage and high morbidity and mortality rates. A surgical or drug-induced blockage of renal sympathetic nerve prevents, partially, the development of IR-induced AKI. Modulation of the Cholinergic Anti-Inflammatory Pathway (CAP) by Vagal Nerve Stimulation (VNS) has also a delayed but effective impact in renal IRI. However, the combined effect of renal sympathectomy and VNS had not been well investigated.

**Objectives:** This work aimed at investigating the combined effect of VNS and Renal Denervation (RDN) in preventing deleterious effects of IRI in rats compared to the effects obtained by RDN alone and to elucidate the possible mechanisms.

**Methods:** 32 adult male albino rats were equally allocated into four groups, sham group, IRI group, RDN group subjected to RDN before IRI and a group subjected to RDN and VNS before IRI.

**Results:** Compared to the sham group, renal IRI led to the elevation of BUN, serum creatinine and MDA levels, it also elevated TNF $\alpha$  and reduced GPX activity and nitrate levels in the renal tissue. In addition, IRI lowered BCL2 in the immune-histochemical study and caused renal damage as observed by the histological light and electron microscopic examination. On the other hand, RDN demonstrated partial correction while, a combination of RDN and VNS demonstrated nearly optimum recovery of renal functions, oxidant/antioxidant balance, inflammatory markers as well as marked amelioration of immunohistochemical, structural and ultra-structural studies.

**Conclusion:** VNS augmented and accelerated the renoprotective effects of RDN owing to its antioxidant, anti-inflammatory as well as anti-apoptotic effects. Additionally, when VNS was combined to RDN, the protection against acute renal failure induced by IRI was rapid and effective.

**Keywords:** Acute kidney injury; Ischemia-reperfusion injury; Renal denervation; Vagus nerve stimulation

### Introduction

Acute Kidney Injury (AKI) is commonly associated with high mortality and morbidity and may lead to Chronic Kidney Disease (CKD) and End-Stage Renal Disease (ESRD) [1-3]. AKI is a major consequence of ischemia-reperfusion injury due to decreased arterial and venous blood flow which results in cellular death due to the depletion of energy stores and toxic metabolite accumulation. However, restoration of blood flow and re-oxygenation of the ischemic tissue may paradoxically exacerbate the injury [4,5].

Actually, re-oxygenation to a previously hypoxic tissue is the basic mechanism for the formation of reactive oxygen species [6]. Consequently, multiple enzyme systems including proteases, nitric oxide synthases, phospholipases, and endonuclease are induced and stimulated causing cytoskeleton disruption, membrane damage, DNA degradation, and eventually cell death [7].

AKI is a clinical syndrome characterized by abrupt and sustained decline in glomerular filtration rate resulting in the accumulation of urea and other chemicals in the blood. The neuro-immunological interaction maintains homeostasis and ameliorates responses to stressful conditions and injury. Fast nerve conduction can essentially modulate inflammation [8]. One of the nervous reflexes that modulate inflammation is the Cholinergic Anti-Inflammatory Pathway (CAP). Such pathway modifies innate and adaptive immunity mainly with the spleen,

and modulation of this reflex by Vagus Nerve Stimulation (VNS) is effective in different inflammatory diseases. Therefore, cholinergic signals derived by VNS provide continuous nervous regulation of cytokine synthesis, which limits the magnitude of the inflammatory immune response and mediates protective effect against AKI induced by IRI [9].

Nevertheless, protection against renal IRI by VNS was found to be time-limited and at least 24 hours prior to IRI was needed for VNS to elucidate its protective effect [8]. The limited and/or delayed response of VNS might be due to stimulation of renal sympathetic innervations through a vagosympathetic reflex [10]. Over activity of renal sympathetic nerves is common in kidney injury which may lead to glomerulonephritis and may induce proteinuria through and beyond its effect on blood pressure [11].

Renal Denervation (RDN) simultaneous to injury improves histology and decreases proinflammatory, profibrotic, and apoptotic changes in the kidney [12]. Therefore, we suppose that RDN may confer added and fast protective effect to VNS against renal IRI. Thereby, in this study, we hypothesize that RDN would protect the kidney and might potentiate or accelerate the renoprotective effects of VNS in a rodent model of AKI induced by IRI in a trial to elucidate such protective impacts and to investigate their possible mechanisms.

## Material and Methods

This work was performed on adult male Wistar rats; initially weighing 150 g to 220g, Rats were obtained from the laboratory animal colony, Ministry of Health and Population, Helwan, Cairo, Egypt and maintained in the animal house of the Medical Ain Shams Research Institute (MASRI) under standard conditions of boarding. Rats were kept at room temperature ( $25^{\circ}\text{C} \pm 5^{\circ}\text{C}$ ) under a 12 hour light/dark cycle. The rats were provided with a regular diet consisting of bread, vegetables, and milk. Tap water was provided ad libitum.

## Experimental Design

After acclimatizing for 7 days, the animals were divided into four groups (with 8 rats each)

Group I, Sham control group: underwent the same procedure of other groups without clamping of the arteries, renal denervation or vagal nerve stimulation

Group II, Ischemia-Reperfusion (IR) group: subjected to bilateral clamping of renal pedicles for 40 min followed by reperfusion for 24 hours.

Group III, Renal Denervation (RDN) group: subjected to bilateral renal denervation prior to bilateral renal IR by the same protocol of the IR group.

Group IV, Vagal Nerve Stimulation (RDN-VNS) group: underwent RDN followed by VNS 10 min before bilateral renal IR as in group II.

## Experimental Procedure

### Renal denervation (RDN)

Rats of the RDN group and RDN-VNS groups were anesthetized with an (i.p.) injection of ketamine (120 mg/kg) and xylazine (12 mg/kg). An abdominal approach to the kidneys was used, with a midline incision then displacing abdominal content to gain access to each kidney one by time. Both kidneys underwent removal of the covering capsule to grant the removal of suprarenal glands and better denervation. Then nerves running along with the renal artery through renal pedicle were surgically removed [12]. 10 min later, bilateral renal artery clamping was performed for 40 min and ischemia was ensured visually by pale-colored kidneys as well as by loss of arterial pulsation.

### Vagal nerve stimulation (VNS)

Rats of RDN-VNS group were subjected to RDN followed by VNS by the following technique: A midline cervical incision was made to expose the left vagus nerve which then placed on a bipolar silver wire electrode for stimulation. Electrical stimulation (50  $\mu\text{A}$  intensity; frequency, 5 Hz; duration, 1 ms) was applied for 1 minute using an isolated square wave stimulator [8,13]. The left vagus nerve was selected because it is commonly used for experimental stimulation in animals and humans [14-16]. 10 min later, bilateral renal artery clamping was performed for 40 min and ischemia was ensured visually by pale-colored kidneys as well as by loss of arterial pulsation. In sham-operated animals, the same technique of vagus nerve exposure was made but was not stimulated and the kidneys were exposed also but not underwent IR technique.

### Renal Ischemia/reperfusion injury

The skin of the anterior abdominal wall was sterilized by tincture iodine, a midline incision was performed, and the abdominal wall was retracted. Both renal pedicles were clamped off by atraumatic clamps for 45 min with a continuous intraperitoneal dropping of saline to inhibit dryness of the kidneys. Pale kidneys by inspection indicated successful clamping, followed by 24 h of reperfusion [17]. After clamp removal, the kidneys were inspected for a change in color from pallor to flushing within 3 min to ensure reperfusion. The abdominal wall was closed with 3-0 silk after homeostasis and the local application of broad-spectrum antibiotic.

## Anesthesia

After 24 hours of reperfusion, overnight fasted rats were weighed and injected intraperitoneally with 5000 IU/Kg B.W heparin sodium (Nile Company, Egypt). Fifteen minutes later, the rats were anesthetized with I.P. injection of thiopental sodium (Sandoz, Austria), in a dose of 40 mg/kg B.W.

## Blood and Tissue Sampling

Blood samples were collected from retro-orbital plexus with the help of capillary tube into serum gel tubes which were centrifuged (6000 rpm for 15 min) to separate serum. The serum was then pipetted into clean storage tubes and stored at  $-20^{\circ}\text{C}$  for later determination of serum urea, creatinine, and MDA. Whereas, left kidneys were stored at  $-80^{\circ}\text{C}$  for later determination of renal tissue GPX and renal tissue nitrate and renal tissue  $\text{TNF}\alpha$  as well. On the other hand, right kidneys were divided into 2 halves; one of them was stored in 10% formalin for later light microscopic examination while the other half was stored in glutaraldehyde for E/M examination.

## Biochemical Analysis

Serum urea, creatinine and Malon-Di-Aldehyde (MDA) were estimated according to the methods described by Patton and Crouch [18], Bartels et al. [19] and Draper and Hadley [20] respectively, using kits supplied by Biodiagnostic, Egypt. The BUN is calculated as  $28/60$  or  $0.446$  of the blood urea.

## Biochemical Analysis in Renal Tissue

Left kidney homogenate (10%, w/v) was prepared with 0.1 M PBS and centrifuged at 12,000 g for 10 min. The supernatant was used to determine GPX levels by the colorimetric method according to Paglia and Valentine [21], using kits supplied by Bio-diagnostic, Egypt. Tissue tumour necrosis factor- $\alpha$  ( $\text{TNF}\alpha$ ) was performed with 'sandwich' enzyme-linked immunoadsorbent assay (ELISA) using a commercially available Mouse  $\text{TNF}\alpha$  DuoSet kit (Genzyme Diagnostics, Cambridge, MA) [22] while nitrate, the metabolic end product of nitric oxide (NO) was assayed according to Bories and Bories [23].

## Histological and Immunohistochemical Studies

One half from right kidney was processed for histological examination by light microscope, the kidney specimens were fixed in 10% neutral buffered formalin and paraffin blocks were prepared. Serial 4-6  $\mu\text{m}$ -thick sections were cut and stained by Hematoxylin and Eosin (H & E), Masson trichrome (MT) stain and BCL2 immune reaction. Another half from right kidney was divided into 2 parts, one (1/4 kidney) processed for transmission electron microscopic examination, small kidney specimens (1 mm<sup>3</sup>) were fixed in a 4% glutaraldehyde solution. Ultrathin sections were cut and examined using a 1200 EX Jeol, Japan, transmission electron microscope at the Electron Microscopic Unit-Faculty of Science, Ain Shams University. The second part (1/4 kidney) was placed on the ice quickly and homogenized with lysis buffer. Aliquots were stored in a  $-70^{\circ}\text{C}$  refrigerator with sodium orthovanadate (2 mM), phenylmethylsulfonyl fluoride (0.2 mM), leupeptin (2  $\mu\text{g}/\text{mL}$ ), and aprotinin (2  $\mu\text{g}/\text{mL}$ ) on ice for 30 min, then were centrifuged at 13,000 g for 15 min at  $4^{\circ}\text{C}$ . Proteins from homogenization (50  $\mu\text{g}$  protein) were electrophoretically separated by 8% or 12% SDS-PAGE and then transferred onto the nitrocellulose membrane. After blockade of

non-specific sites with 5% none fat milk for 1 h at room temperature, membranes were incubated with a rabbit polyclonal anti-CTGF, AKT/PKB.

## Immunohistochemical BCL2 Study

BCL2 immunohistochemical (anti-apoptotic protein) evaluation was carried out as previously described by Bancroft et al. [24]. Five mm tissue sections were deparaffinized and rehydrated in gradient alcohols and processed using the streptavidin immunoperoxidase method. In brief, sections were submitted to antigen retrieval by microwave oven treatment for 10 min in 0.01 mol/L citrate buffer (pH 6.0). Slides were then incubated in 10% normal serum for 30 min, followed by overnight incubation at 4 with the appropriately diluted primary Bcl2 antibody (Beyo time Inc., China) were used at 1:100 dilution. Next, samples were incubated with biotinylated anti-rabbit immunoglobulins for 15 min at  $37^{\circ}\text{C}$ . Then, they were incubated with streptavidin-peroxidase complexes for 15 min at  $37^{\circ}\text{C}$ . After rinsing in PBS, the reaction products were observed by immersing the section into the chromogen diaminobenzidine. Finally, counterstaining of the sections with Mayer's hematoxylin was done followed by dehydrating and mounting. The negative control was processed in the same way, but omitting the step of 1ry Ab. The positive cells showed brown nuclei reaction.

## Statistical Analysis

The data collected, tabulated and statistically analyzed, using statistical package for social science (SPSS) 22.0 for windows (SPSS Inc., Chicago, IL, USA). A p-value  $<0.05$  was considered significant. Continuous variables were expressed as mean, standard deviation (SD) and median, checked for normality by using Shapiro-Wilk test. One way (ANOVA) F test used for comparison between more than two groups, with Holm Sidik methods for multiple comparisons, Kraskall Wallis test was used to compare between more than two groups of non-normally distributed data, with Turkey methods for multiple comparisons. Pearson's correlation was calculated to assess the correlations between various study parameters. (+) sign indicate positive correlation and (-) sign indicate negative correlation.

## Results

In our study, there was a significant elevation in the renal function tests of the IR group compared to the sham control group (BUN  $p<0.001$ , serum creatinine  $p<0.05$ ). A significant decrease of BUN level was observed in the RDN group compared to the IR group ( $p<0.001$ ) while non-significant difference was found between both groups regarding serum creatinine level ( $p=0.09$ ). Though, the BUN levels remained significantly higher in the RDN group compared to sham controls ( $p<0.001$ ) but serum creatinine was nearly normalized and showed no significant difference between both groups.

A significant reduction was found concerning the renal function tests of the RDN-VNS group compared to that of the IR group (BUN  $p<0.001$ , serum creatinine  $p<0.05$ ) becoming comparable to the sham control group.

Moreover, a significant reduction of renal tissue nitrate levels and significant increase of renal tissue TNF $\alpha$  were noticed in the IR group as compared to the sham control group ( $p < 0.001$  for both parameters). On the other hand, Renal tissue nitrate levels in RDN group demonstrated a significant elevation in comparison to the IR group ( $p < 0.001$ ) and remained significantly decreased when compared to the sham control group ( $p < 0.001$ ). Whereas, no significance was found regarding renal tissue TNF $\alpha$  levels in the RDN group compared to the IR group, while significantly elevated compared to the sham control group ( $p < 0.001$ ). As regards the RDN-VNS group, a significant increase was found in the levels of renal tissue nitrate compared to the IR group ( $p < 0.001$ ), but became normalized when the RDN-VNS group was compared to the sham control group. Similarly, a significant decline of renal tissue TNF $\alpha$  levels in RDN-VNS was observed compared to the IR group ( $p < 0.001$ ), becoming non-significant when compared to the sham control group.

Regarding oxidative/antioxidant biomarkers, a significant rise of serum MDA and decline of renal tissue GPX enzyme activity levels were found in the IR group compared to the sham control group ( $p < 0.001$ ), while a significant decline of GPX

enzyme activity was demonstrated in the renal tissue GPx levels of IR group compared to sham group ( $p < 0.001$  for both). Serum MDA levels in the RDN group were significantly lower than that of the IR group ( $p = 0.005$ ) but remained significantly elevated compared to the sham control group ( $p < 0.001$ ). On the other hand, renal tissue GPx levels of the RDN group were comparable compared to IR and sham groups.

A significant decrease of serum MDA levels of the RDN-VNS group compared to that of the IR group ( $p < 0.001$ ) and became comparable to the sham control level. Likewise, a significant increase was found regarding renal tissue GPx levels of the RDN-VNS group compared to that of the IR group ( $p < 0.001$ ) but none significant compared to the sham control group (**Table 1**).

Regarding correlation studies among studied groups, S.MDA and renal tissue TNF $\alpha$  showed significant positive correlation with (BUN and S. creatine) and significant negative correlation with renal tissue nitrate. On the other hand, renal tissue GPx enzyme activity showed significant negative correlation with (BUN and S. creatine) and significant positive relationship with renal tissue nitrate level (**Table 2**).

**Table 1:** Mean  $\pm$  Standard deviation (SD) of BUN, Serum creatinine, Renal tissue nitrate, Serum MDA, and Renal tissue GPx in the different studied groups.

		BUN (mg/dL)	Serum creatinine (md/dl) [8]	Renal tissue Nitrate (pmol/g) [8]	Renal tissue TNF $\alpha$ (pg/ml) [8]	Serum MDA ( $\mu$ mol/L) [8]	Renal tissue GPx (U/mg) [8]
Sham (8)	Mean $\pm$ SD	18.762 $\pm$ 1.871	0.9357 $\pm$ 0.2389	95.25 $\pm$ 6.18	17.041 $\pm$ 2.699	1.638 $\pm$ 0.478	3.15 $\pm$ 0.428
IR (8)	Mean $\pm$ SD	44.15 $\pm$ 5.78	3.319 $\pm$ 0.687	46.25 $\pm$ 9.35	30.31 $\pm$ 3.38	4.85 $\pm$ 0.51	1.775 $\pm$ 0.495
	P <sup>1</sup>	<0.001*	<0.0*	<0.001*	<0.001*	<0.001*	<0.001*
RDN (8)	Mean $\pm$ SD	34.32 $\pm$ 4.99	2.006 $\pm$ 0.606	72 $\pm$ 10.03	27.31 $\pm$ 4.78	4.025 $\pm$ 0.456	2.5 $\pm$ 0.428
	P <sup>1</sup>	<0.001*	<0.1*	<0.001*	<0.001*	<0.001*	0.026*
	P <sup>2</sup>	<0.001*	0.09	<0.001*	0.1	0.005*	0.015*
RDN VNS (8)	Mean $\pm$ SD	19.622 $\pm$ 2.767	2.006 $\pm$ 0.606	91.63 $\pm$ 9.44	20.32 $\pm$ 2.87	1.85 $\pm$ 0.55	2.888 $\pm$ 0.488
	P <sup>1</sup>	0.683	<0.3	0.421	0.141	0.402	0.264
	P <sup>2</sup>	<0.00*	<0.05*	<0.001*	<0.001*	<0.001*	<0.001*
	P <sup>3</sup>	<0.00*	<0.2	<0.001*	0.001*	<0.001*	0.197
SD: Standard deviation							
In parenthesis is the number of observation.							
IR: Ischemia-reperfusion Injury group							
RDN: Renal denervation-ischemia-reperfusion injury group							
RDN-VNS: Renal denervation+vagal nerve stimulation group							
P <sup>1</sup> : significance from sham group							
P <sup>2</sup> : significance from the IR group							
P <sup>3</sup> : significance from RDN group							

P: values are obtained using (t-test type)

**Table 2:** Correlation between kidney function tests (BUN, Serum creatinine), renal tissue nitrate levels and serum MDA, renal tissue GPx and serum TNF $\alpha$  in different studied groups.

		S MDA ( $\mu\text{mol/L}$ )	Renal tissue GPx (U/mg)	S TNF $\alpha$ (pg/ml)
BUN (mg/dL)	r	0.91	-0.62	0.83
	P#	<0.001	<0.001	<0.001
S. creatine (mg/dL)	r	0.82	-0.74	0.72
	P#	<0.001	<0.001	<0.001
Renal tissue nitrate (pmol/g)	r	-0.83	0.71	-0.7
	P#	<0.001	<0.001	<0.001

#: Pearson correlation, the sign before (r) represent the direction of correlation, while P represents the significant of correlation, P considered significant if < 0.05.

## Histological Results

### H and E-stain: Control (sham) group: (Figure 1A-1D)

Examination of H and E-stained sections obtained from the kidney of the control (sham) rats revealed average cortical thickness, average medullary thickness and intact renal capsule (Figure 1A). A normal histological structure of the renal cortex showed average Malpighian renal corpuscles which were composed of the glomerulus (a tuft of blood capillaries) surrounded by Bowman's capsule with capsular space in between. The parietal layer of the capsule had a single layer of simple squamous cells, whereas the visceral layer was lined by podocytes with oval nuclei, surrounded by average proximal tubule were lined by three to five pyramidal cells characterized by acidophilic cytoplasm, apical brush border of microvilli, and rounded, vesicular, basally located, basophilic nuclei with free lumens and distal tubules were lined by six to eight cubical epithelial cells with a wider lumen. The cells of the DCT have pale acidophilic cytoplasm and rounded, centrally situated, vesicular, basophilic nuclei with free lumens and collecting tubule and interstitium contain average blood vessels and intact renal capsule (Figure 1B and 1C). Also, average renal medulla showing average collecting tubules, lined by cuboidal cells had very pale acidophilic cytoplasm with free lumens, and average intervening stroma containing normal blood vessels were observed (Figure 1D).

### Renal ischemia-reperfusion (IR) group: (Figure 2A-2D)

The H and E stained sections of the rat kidney in this group revealed that, thin cortical thickness in relation to medulla together with medullary rarefaction at focal areas and partially detached renal capsule (Figure 2A). The cortical area by the high power of magnification showed renal corpuscle with shrunken, markedly distorted and congested small glomeruli have a

widened bowman's space and the abnormal configuration of renal tubules were observed. In some proximal and distal tubules showed the cytoplasm of some lining cells rarefied exhibiting cytoplasmic vacuoles, epithelial exfoliation at focal areas of some tubules. Flattening of the epithelial lining of some tubules with apparent tubular dilatation and few were destructed and degenerated but few of them were average. Also, homogenous materials, Cellular debris is dislodged within their lumina and congested in more than 60%. Dilated congested blood vessels were also observed (Figure 2B).

All stained sections showed necrotic changes in the majority of the cortical tubular epithelial cells in the form of pyknotic and karyolytic nuclei, in addition to vacuolation. Interstitial inflammatory mononuclear cellular infiltrations were noticed (Figure 2C).

Also, medullary area showed mononuclear cellular infiltration between disorganized degenerated tubules in addition to peritubular congestion (Figure 2D).

### RDN group: (Figure 3A and 3B)

The H and E stained renal sections showed renal cortex with some of the renal corpuscles, glomeruli and Bowman's spaces looked average in size and shape but others showed slightly congested glomeruli and little widening of Bowman's space. Also, some tubules seemed free from exfoliation in their luminae but others contained exfoliation in their luminae and intracellular cytoplasmic vacuoles. In addition, some of the blood vessels were dilated and moderately congested and few of the mononuclear cells infiltrated in the interstitium (Figure 3A). The medullary area showed mononuclear cellular infiltrations in the interstitium of average tubules but some of them showed exfoliated cell debris and homogenous materials in their lumina and some pyknotic nuclei in their lining epithelium. Slightly dilated congested blood vessel was also observed (Figure 3B).

### RDN-VNS group: (Figure 4A-4D)

The H and E stained renal sections showed an average diameter of cortex and medulla with average glomeruli and tubules covered by an intact capsule (Figure 4A). Higher

magnification showed that most of the renal corpuscles were intact as the glomeruli were normal and Bowman's capsules were patent. Proximal, distal and collecting tubules were also normal. The rest showed slightly wide Bowman's space and some of the tubules contained few pyknotic nuclei and cytoplasmic vacuoles. Few mononuclear cellular infiltrations in the interstitium were also observed (**Figure 4B**).

Renal medulla showed that most of the tubules were normal but some of them were dilated, with average epithelial lining. Most of the nuclei were rounded and vesicular, but few of them were flat and pyknotic. A very little number of mononuclear cellular infiltration in the interstitium was noticed (**Figure 4C**). Renal medulla was with average tubules. Some of the dilated collecting tubules showed the average epithelial lining. Most of their nuclei were rounded vesicular, but few of them were flat and pyknotic. A scanty mononuclear cellular infiltration in the interstitium could be observed (**Figure 4D**).

## Masson's Trichrome Stain

### Sham group

The renal cortex showed very thin blue collagen around Bowman's capsules and renal tubules (**Figure 5A**).

### IR group

The renal cortex showed a marked increase of the collagen fibers around the Bowman's capsules and the capillary loops of glomeruli, mononuclear cellular infiltrations and the tubules (**Figure 5B and 5C**). Renal medulla showed a marked increase of the collagen fibers around mononuclear cellular infiltrations, tubules; septa between tubules (**Figure 5D**).

### RDN group

The renal cortex showed few collagen fibers around the renal capsules, the glomeruli, and the tubules. Also, septa between tubules were intact in comparison to IR group (**Figure 5E**).

### RDN-VNS group

The renal cortex and medulla showed minimal collagen fibers around the Bowman's capsules and the tubules (**Figure 5E and 5F**).

## BCL2

### sham-operated group

The renal cortex showed positive immunoreactions of the nuclei in renal corpuscle and nuclei among the tubular lining cells (**Figure 6A**).

### IR group

The renal cortex showed weak immunoreactions of the nuclei in glomeruli, Bowman's capsule and among the tubular lining cells (**Figure 6B**).

### RDN group

The renal cortex showed moderately positive immunoreactions of the nuclei in glomeruli, Bowman's membrane and among the lining tubular epithelial cells compared to IR group (**Figure 6C**).

### RDN-VNS group

The renal cortex showed markedly positive immunoreactions of the nuclei in glomeruli, Bowman's membrane and among the lining tubular epithelial cells compared to the IR group (**Figure 6D**).

## EM

### Sham group: (Figure 7A-7C)

Examination of ultrathin sections showed that podocytes had primary long processes which branched giving secondary processes which produced feet processes or pedicles with narrow slits (bridged by a slit membrane) in between. The podocytes and glomerular capillaries shared a uniform thickness of a basement membrane which exhibited a trilaminar composed of a central electron-dense layer (lamina densa) and two electron-lucent layers (lamina rarae) on either side. The podocytes contained a large irregular euchromatic indented nucleus with peripheral dense chromatin. The fenestrated endothelial lining of the glomerular blood capillaries was noticed (**Figure 7A**). The proximal tubules demonstrated high cubical cells and showed apical condensed microvilli and basal numerous enfolding enclosing elongated mitochondria with normal cristae. The cytoplasm contained some small pinocytic vesicles and few lysosomes. The large euchromatic nuclei with peripheral chromatin condensations were noticed (**Figure 7B**).

The distal convoluted tubules were lined by cubical cells which appeared smaller than those of the proximal ones, with few short microvilli and large rounded euchromatic nuclei near to their luminal surface with peripheral chromatin condensations. The cells of the tubule were separated from the delicate capillary by the basement membrane. The cytoplasm contained a few and small pinocytic vesicles and few lysosomes. The large numbers of elongated mitochondria with normal cristae were located basally in the cells between basal enfolding (**Figure 7C**).

### IR Group (Figure 8A-8D)

The podocytes showed the 1ry process with elongated irregular nuclei. The other cells had shrunken, heterochromatic and pyknotic nuclei. Also, they showed disorganization, distortion, and fusion in the feet processes. Irregular thickening of glomerular basement membranes was clearly seen. Dilated glomerular capillaries with lack of fenestrations and mesangial cells and their surrounding thick amorphous mesangial matrix were observed. Marked irregular thickening of Bowman's membrane surrounded by a thick layer of collagen fibers was also an observation (**Figure 8A**).

The proximal tubular cells showed variable ultrastructural changes. Some cells had disoriented basal mitochondria, with few and dilated basal enfolding as well the presence of multiple vacuoles. Many cells showed dilated perinuclear space. Multiple secondary lysosomes, disconfigured mitochondria, and electron-dense bodies could be observed in the cellular cytoplasm (**Figure 8B**). The proximal tubular cells contained also areas of rarified cytoplasm, swollen mitochondria with ill-defined cristae. Many dense irregular bodies mostly lysosomes were found. Heterogenous, pleomorphic, autophagic vacuoles containing whorls of membranous material were also observed. There were shrunken, condensed pyknotic nuclei, while the microvilli were mostly dilated and irregular together with irregular thickened basal laminae were detected (**Figure 8C**).

The cells of the distal convoluted tubule demonstrated that the majority of the cells with few basal enfolding and a palisade form of the mitochondria but their cytoplasm showed some rarefaction. On the other hand, some atrophied tubules with irregular thickening of the basement membranes surrounded by hemorrhagic areas and thick collagen fibers in between the tubules. The cells revealed shrunken condensed and/or pyknotic nuclei, but others had completely atrophied nuclei. Large areas of rarified cytoplasm with disorganized and dilated basal enfolding were shown. The mitochondria were swollen and directed towards the lumen with loss of their parallel arrangement in addition to the observation of indistinct cristae and obliteration of tubular lumen (**Figure 8D**).

## RDN Group (Figure 9A-9C)

The podocytes showed disorganized pedicles and electron-dense substances in the glomerular capillaries. The mesangial cells were surrounded by mesangial matrix. Thick regular Bowman's capsule with a thin layer of collagen was visible on the outer aspect of the basal lamina. The blood capillaries and red blood corpuscles were noticed (**Figure 9A**).

Lumens of the proximal tubules were filled with secretions. The lining cells of the tubules showed microvilli, small cytoplasmic vacuoles, and small dense lysosomes but some of their mitochondria were swollen (**Figure 9B**).

The cells of the distal tubules revealed small lysosomes and some elongated mitochondria with mostly intact cristae. Areas of cytoplasmic rarefaction could be observed. Some nuclei were irregular in shape and shrunken, but others were nearly average in appearance. The brush borders couldn't be detected but basal enfolding and thickening could be observed at some of the basal laminae (**Figure 9C**).

## RDN-VNS Group :(Figure 10A-10C)

The podocytes showed euchromatic indented nuclei and mitochondria and few small vacuoles were seen in their cytoplasm. They appeared with normal arranged secondary feet processes. The space between the pedicles (filtration slits) could be seen and laid on a regular glomerular basement membrane. Glomerular capillaries lacking fenestrae were seen. Though, some of the podocytes showed distorted and fused feet

processes with the appearance of a few mesangial matrixes around mesangial cells (**Figure 10A**).

The cells of the proximal tubules revealed long, dense apical microvilli and basal enfolding in addition to the presence of small pinocytotic vesicles near to the lysosomes. Many elongated mitochondria with distinct cristae and large nuclei with peripheral condensed chromatin could be observed (**Figure 10B**).

The cells of the distal tubules revealed elongated mitochondria with mostly intact cristae. Small areas of cytoplasmic rarefaction could be observed. Most of the nuclei were normal in appearance, but scanty of them revealed pyknotic. The brush borders couldn't be detected but basal enfolding could be observed in some areas. Little thickening of the basement membrane and very small vacuoles were noticed (**Figure 10C**).

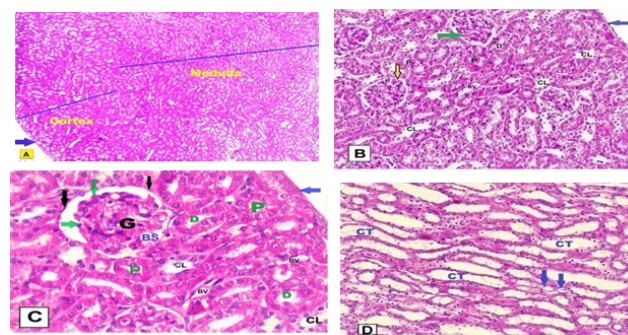


**Figure 1:** Photomicrograph of a section in the rat kidney of control (sham) group stained with H & E showing: A: renal tissue with average thickness of the cortex and medulla with intact renal capsule (blue arrow) (x40); B: Renal cortex containing Malpighian renal corpuscles with average glomeruli (green arrow), average Bowman's space (yellow arrow) and intact Bowman's capsule (blue arrow). Also, proximal tubules (P), distal tubules (D), collecting tubules (CL) are average and interstitium contains blood vessels (BV) in between them. Part of the intact renal capsule could be detected (blue arrow) (x200); C: Renal cortex with normal Malpighian renal corpuscle containing average of the glomerular capillary tufts (G), with average cellularity surrounded by Bowman's space (BS), and patent Bowman's capsule with flat epithelium lining (black arrow) surrounded by normal shaped proximal tubule (P) lined by pyramidal cells having apical brush border, rounded basal vesicular nuclei and free lumens and distal tubules (D) are lined by cubical cells having rounded central vesicular nuclei with free wide lumens and collecting tubule (CL). Part of the patent renal capsule (blue arrow) can be observed. Note acidophilia of proximal and distal tubular cells (x400); D: Normal renal medulla showing average collecting tubules (CT) with free lumens, and average intervening stroma containing normal blood vessels (blue arrows) (x400).

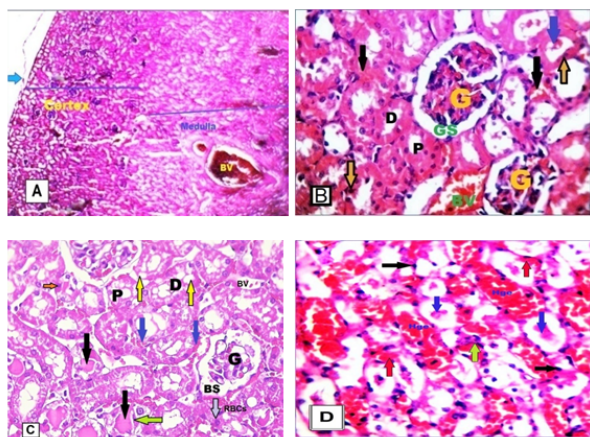


**Figure 2:** Photomicrograph of a section in the rat Kidney of renal ischemia-reperfusion (IR) group stained with H and E showing: A: Thin cortical thickness in relation to the medulla. Focal areas of medullary rarefaction and partially detached renal capsule (blue arrow) and dilated congested blood vessels (BV) can be observed (x40); B: Cortical area showing two Malpighian corpuscles with shrunken markedly distorted congested glomeruli (G) having a widened bowman's space (BS) and abnormal configuration of renal tubules. In some proximal (P) and distal (D) dilated tubules the cytoplasm of some lining cells was rarefied exhibiting vacuoles (yellow arrows) and pyknotic nuclei. Also, Cellular debris (green arrow) is dislodged in the tubular lumina and haemogenous materials (black arrow). Interstitial mononuclear infiltration (gray arrow) and red blood corpuscles (RBCs) are noticed (x400); C: Cortical area showing two Malpighian renal corpuscles with marked distorted congested glomeruli (G) and widened Bowman's space (BS), congested dilated interstitial blood vessels (BV), exfoliation of some lining epithelial cells of some tubules (blue arrow), flattening of the epithelial lining of some tubules (red arrow). Some tubular cells showed vacuolated cells (black arrow) with pyknotic nuclei (yellow arrows). Inflammatory cells infiltration in the interstitium (green arrow) are noticed and peritubular congestion could be seen (red arrows) (x400); D: medullary area showing mononuclear cellular infiltrations (green arrow) and peritubular congestion could be seen (red arrows) (x400).

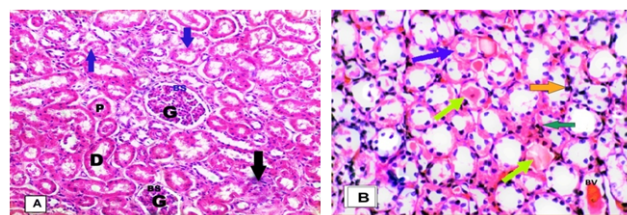


**Figure 3:** Photomicrograph of a section in the rat Kidney of renal denervation (RDN) group stained with H and E (x200) showing A: renal cortex with average Malpighian renal corpuscle having average glomeruli (G) Bowman's space (BS), proximal (P) and distal (D) tubules, some of them containing exfoliated materials in their luminae (blue arrow) in addition to the presence of few infiltrating inflammatory cells (black arrow) in interstitium could be seen; B: Renal medulla showed focal areas of mononuclear cellular infiltrations in interstitium (green arrow), average tubules but some of them show exfoliated cell debris and homogenous materials in their luminae (yellow arrow) and some pyknotic nuclei in their lining epithelium (red arrow). The slightly dilated congested blood vessel can be also observed.

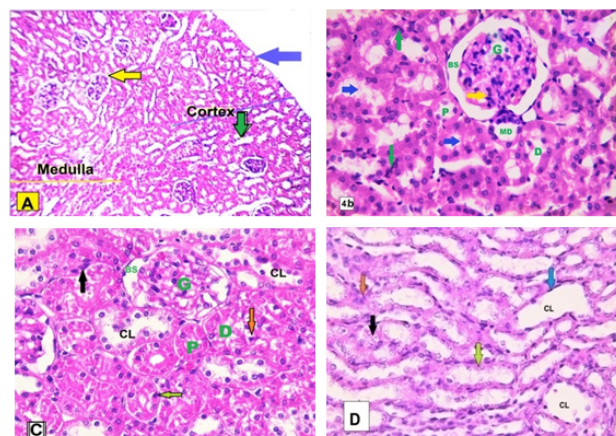


**Figure 4:** Photomicrograph of a section in the rat kidney in vagal nerve stimulation (RDN-VNS group) stained with H and E showing A: average diameter of cortex and medulla with average glomeruli (yellow arrows), and tubules (green arrow) covered with intact capsule (blue arrow) (x100); B: Renal cortex with renal corpuscle containing average glomeruli (G) slightly widened patent Bowman's space (BS), average proximal (P), distal (D) and collecting tubules (CL); C: Some of them contain few pyknotic nuclei (green arrow) and few of cytoplasmic vacuoles (red arrows) in their lining cells. Few of the mononuclear cellular infiltration in the interstitium (black arrow) can be observed (x400); D: Renal medulla with average tubules. Some of the dilated collecting tubules (Cl) showing average epithelial lining, most of the nuclei are rounded vesicular (green arrows), but few of them are flat and pyknotic (blue arrow). There were few mononuclear cellular infiltrations in the interstitium could be observed (x400).

## Masson Tri-Chrome Stain

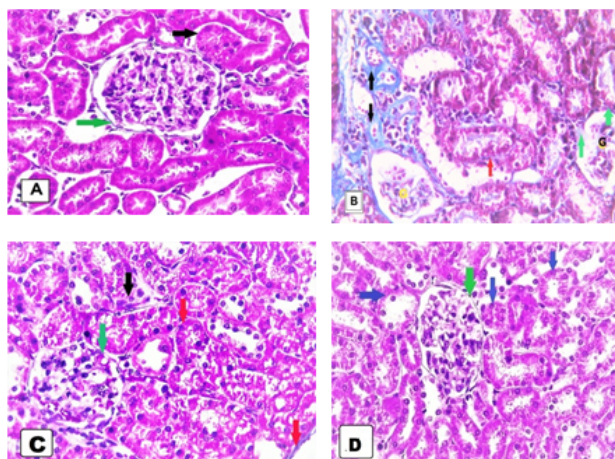


**Figure 5:** Photomicrograph of a section in the rat renal tissue from all groups stained by Masson's Trichrome (x400) showing A: sham group: thin blue collagen around renal tubules (black arrow), Bowman's capsules (green arrow); B: In I/R group: The renal cortex with a marked increase of the collagen fibers around mononuclear cellular infiltrations (black arrows), convoluted tubules (red arrow), Bowman's capsules (green arrow) and capillary loops of the glomerulus (G); C: IR group: renal medulla with a marked increase of the collagen fibers around mononuclear cellular infiltrations (green arrow), tubules (blue arrow) and septa between tubules (red arrow); D: RDN group showed renal cortex with few collagen fibers around glomeruli (G) and convoluted tubules (red arrow). It showed also interstitium (black arrow) and part of the renal capsule (yellow arrow).

## Immunohistochemical Study of BCL2 Reaction

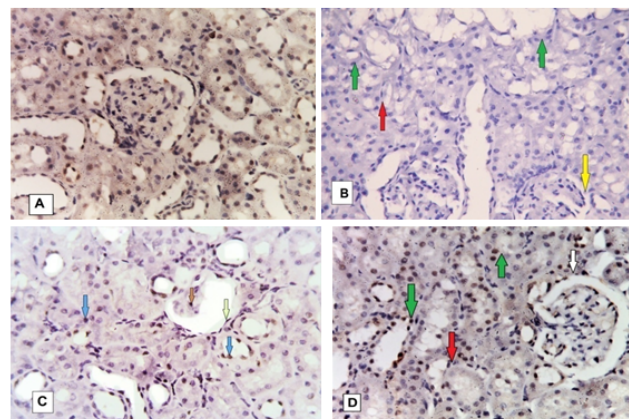


**Figure 6:** Photomicrograph of a section in the renal cortex of a rats of all groups for immunohistochemical reaction of BCL2 (x400) showing A: sham group, positive immunoreactive nuclei (red arrows) among the tubular lining cells; B: IR group, a weak immunoreactive nuclei in glomeruli (red arrows), Bowman's capsule (green arrow) and among the tubular lining cells (blue arrows); C: RDN group, moderately positive immunoreactive nuclei in glomeruli, Bowman's membrane (green arrow) and among the lining tubular epithelial cells (blue arrows) compared to IR group; D: RDN-VNS group, markedly positive immunoreactive nuclei in glomeruli (white arrow), Bowman's membrane (red arrow) and among the lining tubular epithelial cells (blue arrows).

## Electron Microscopic Examination

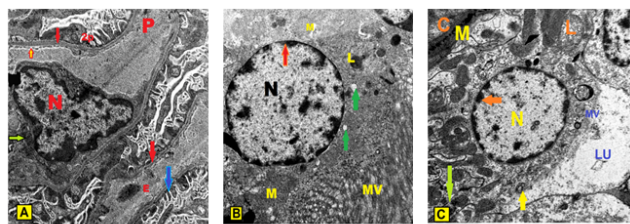


**Figure 7:** An electron micrograph of a section of the renal cortex of a rat in sham group showing A: Podocytes with large irregular euchromatic indented nucleus (N) with peripheral dense chromatin. The podocyte appears with the primary process (P) and secondary interdigitating feet processes or pedicles (red arrow). The space between the feet or pedicles called filtration slits. The fenestrated endothelial lining of blood capillary (Yellow arrow) could be also noticed. Uniform thickness of glomerular basement membrane (GBM) is observed (blue arrows) and a central electron dense lamina densa and lamina rare on either side are also detected. Mesangial cells (green arrows) are also noticed (x12000); B: A cell in a proximal convoluted tubule with elongated mitochondria (M) having normal cristae. The brush border of the cells has normal microvilli (MV) and contains some pinocytotic vesicles (green arrow) and lysosomes (L). Note the large nucleus (N) with peripheral chromatin condensations (red arrows) (x12000); C: A part of a DCT which is lined by cubical cells with short few microvilli (MV) and large rounded nucleus (N) near to their luminal surface (LU) with peripheral chromatin condensations (red arrows). The cells of the tubules we separated from the delicate capillary by the basement membrane (C). The cytoplasm contains some pinocytotic vesicles (yellow arrow) and few lysosomes (L). Note a large number of elongated mitochondria (M) with normal cristae situated in the basal parts of the cells between basal enfolding (green arrows) (x10000).

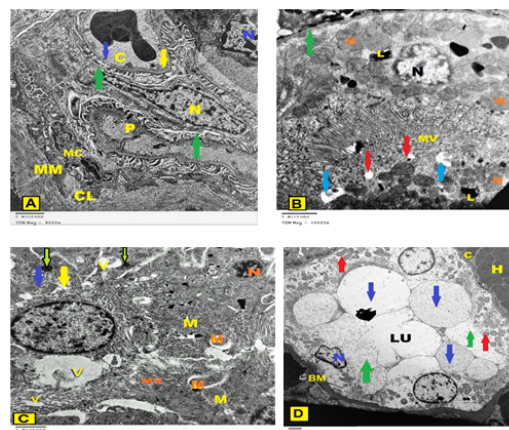


**Figure 8:** An electron micrograph of a section of the renal cortex of a rat IR group showing A: Podocytes with the 1ry process (P) are shown with an elongated irregular nucleus (yellow N). The part of the other cell has a shrunken, heterochromatic and pyknotic nucleus (blue N). Also, they show disorganization, distortion, and fusion of some of the feet processes (green arrow). Irregular thickening of glomerular basement membranes (yellow arrow) is clearly seen. Dilated glomerular capillary (C) with lack of fenestrations (blue arrow) is also found. Mesangial cell (MC) and its surrounding amorphous mesangial matrix (MM) and Marked thickening of Bowman's membrane surrounded by a thick layer of collagen fibers (CL) are observed (x8000); B: A proximal tubular cell contains endoplasmic reticulum, heterogenous pleomorphic autophagic vacuoles containing whorls of membranous material (blue arrows), many lysosomes (L) and shrunken apoptotic nucleus (N). Thickening in basal lamina (green arrow), many of cytoplasmic vacuoles (red arrow) in addition to an area of partial loss of the apical microvilli (MV) and swollen mitochondria (M) with variable sizes were apparent (x10000); C: The epithelial lining cells of the proximal convoluted tubule show areas of rarified cytoplasm (yellow arrow), swollen mitochondria (M) with ill-defined cristae. Numerous dense irregular bodies, mostly lysosomes (green arrow) are observed. Pleomorphic, autophagic vacuoles (V) containing whorls of membranous material and the shrunken condensed pyknotic nucleus (N) were found, while the microvilli (MV) were mostly dilated and irregular could be observed (x8000); D: Some of the lining cells of the distal convoluted tubule have small pyknotic nucleus (N), but others have atrophied nucleus, disorganized basal enfolding with the appearance of swollen mitochondria (red arrows) and obliteration of tubular lumen (LU). Other cell lost most of their organelles and appeared to contain variable-sized large vacuoles (blue arrows). Large areas of rarified cytoplasm (green arrows), thick irregular basement membrane (BM) surrounded by capillary (C) and hemorrhagic area (H) were noticed. Apical microvilli could not be detected (x4000).

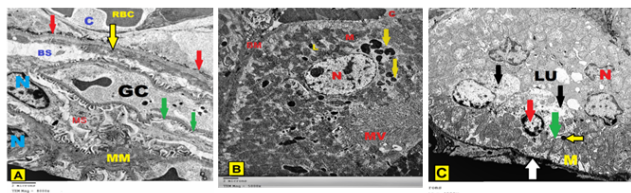


**Figure 9:** An electron micrograph of a renal cortex of a rat in RDN group showing; A: A renal corpuscle with nuclei of podocytes (N), disorganized pedicles (green arrow). Note electron-dense substances (E) in the glomerular capillaries (GC). The mesangial cells (MC) surrounded by a mesangial matrix (MM), thick regular Bowman's capsule (yellow arrow), a thin layer of collagen (red arrows) are visible on the outer aspect of the basal lamina of the Bowman capsule. Cloud capillary (C) and red blood corpuscles (RBCs) are also noticed (x8000); B: A part of proximal tubule and its lumen (LU) filled with secretion, microvilli (MV), small cytoplasmic vacuoles (red arrows), small dense lysosomes (L) average sized mitochondria (M) but some of them are swollen (black arrow) (x8000); C: An epithelial cell of distal tubule revealed small lysosomes (yellow arrow) and some elongated mitochondria (M) with mostly intact cristae. Areas of cytoplasmic rarefaction (black arrow) could be observed. Nuclei (N) are irregular in shape and shrunken, but others (red arrow) are nearly normal appearance. The brush borders couldn't be detected and basal enfolding (green arrow) could be observed in some areas. Thickening of basal lamina (white arrow) is also found (x4000).

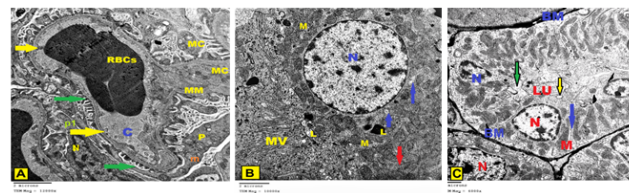


**Figure 10:** An electron micrograph of a renal cortex of a rat from RDN-VNS group showing A: A podocyte (P) with euchromatic indented nuclei (N) mitochondria (m) and few small vacuoles are seen in the podocyte cytoplasm. The podocyte appears with primary and normally arranged secondary feet processes (green arrow). The space between the pedicles (filtration slits) is clearly seen and laid on a regular glomerular basement membrane (yellow arrows). Glomerular capillaries (c) with lack of fenestrations (yellow arrow) are seen. A podocyte (P1) is shown with distorted, fused feet processes. Mesangial matrix (MM) around mesangial cells (MC) is also present (x12000); B: Cells in the proximal tubule reveal long dense apical microvilli (MV), and basal enfolding (red arrow) as well as small pinocytotic vesicles (blue arrow) near to the lysosomes (L). Many elongated mitochondria (M) with distinct cristae are situated. Note the large nucleus (N) with peripheral chromatin condensations. (x10000); C: Epithelial cells of the distal tubule revealed elongated mitochondria (M) with mostly intact cristae. Small areas of cytoplasmic rarefaction (green arrow) could be observed. Some nuclei (red N) are nearly normal in appearance, but few of them (blue N) appear pyknotic. The brush borders couldn't be detected and basal enfolding (blue arrow) could be observed in some areas. Some thickening of the basement membrane (BM) is detected and very small vacuoles (yellow arrow) are noticed (x6000).

## Discussion

The early diagnosis and treatment of acute kidney damage is one of the most important factors in the correction of the progress of this disease. The most well-known methods for early detection of kidney damage are the BUN and serum creatinine levels [25]. IR caused nearly more than 3 fold increase in s. creatinine and more than 2 fold increase in BUN compared to sham group, confirming the development of acute renal failure (ARF) in this model according to RIFLE classification [26] which was proved histologically as the findings in IR rats revealed thin cortical thickening in relation to medulla in addition to the appearance of medullary rarefaction at focal areas and partially detached renal capsule. Some glomeruli were shrunken, markedly distorted and congested having a widened bowman's space and abnormal configuration of renal tubules were observed. Moreover, some proximal and distal tubules showed flattening of the epithelial lining cells, rarefied cytoplasmic vacuoles, epithelial exfoliation at focal areas and apparent tubular dilatation were found. Also, homogenous materials and cellular debris were dislodged within their luminae and dilated congested blood vessels were detected.

Additionally, most of the epithelial cells of cortical tubules were necrotic and their nuclei were pyknotic in addition to the appearance of cortical and medullary interstitial inflammatory mononuclear cellular infiltrations with marked increase of the collagen fibers around the Bowman's capsules. These results were parallel to previous histological studies which revealed severe acute tubular damage in renal sections of the rats subjected to IR [27,28].

Moreover, in the present study, EM examination of kidneys of IR group revealed that the podocytes had 1ry process with elongated irregular nuclei together with disorganization, distortion and fusion in the some feet processes. Other cells showed shrunken, heterochromatic and pyknotic nuclei. Irregular thickening of glomerular basement membranes and dilated glomerular capillaries with lack of fenestrations were clearly seen. Marked irregular thickening of Bowman's membrane surrounded by thick layer of collagen fibers was also observed. Shrinkage of the glomeruli and shrinkage of the capillary network resulting in widening the space between the wall and the network were found in the current study as proved by other study [29].

Additionally, the current study revealed variable ultrastructural changes of the proximal and distal tubular cells. Some proximal convoluted tubular (PCT) cells had disoriented basal abnormal shaped mitochondria, with few and dilated basal enfolding, while, the mitochondria of the distal convoluted tubules (DCT) were found near the lumen with loss of their parallel arrangement. In addition, many cytoplasmic vacuoles, rarified cytoplasm, electron-dense bodies, pyknotic nuclei with dilated peri-nuclear spaces were detected in some tubular cells. Multiple secondary lysosomes, abnormal-shaped mitochondria, and electron-dense bodies could be detected in the cytoplasm of other cells. Additionally, the microvilli of PCT cells were mostly dilated and irregularly thickened basal lamina were detected, while, DCTs showed loss of their microvilli, with shedding of their apical cytoplasm into the lumen. Such findings were in agreement with the result obtained by other authors [30,31].

These findings might indicate that IRI has induced cellular necrosis and/or apoptosis of the tubular cells. The cell swelling and rupture of surface membranes were characteristic for cell necrosis [32]. Inflammatory cell infiltration and cytokine release are frequent consequences of cell necrosis [33] and apoptosis [34].

In our study, there were a wide array of underlying mechanisms including increased oxidative stress as well as, oxidant/antioxidant imbalance as evidenced by the significant rise of serum MDA and decrease of GPX in renal tissue of IR group compared to sham control group. In addition, our work expressed significant positive correlation between s.MDA and BUN and serum creatinine, while it showed significant negative relationship between renal tissue GPX and renal function tests (BUN and serum creatinine). Consistently, it was reported that, [35-38].  $\text{Ca}^{2+}$  overload leads to opening of the mitochondrial transition pore after reperfusion, leading to apoptosis, necrosis and autophagy [39-40]. Also the depressed activity of the antioxidant enzymes such as catalase, superoxide dismutase,

and GPX were found to play a crucial role in the damage of IRI [41].

Additionally, inflammation is also a possible mechanism for renal damage observed in IR rats. This was proved by the significant elevation of renal tissue  $\text{TNF}\alpha$  as an inflammatory marker and significant reduction of the renal tissue nitrate levels.  $\text{TNF}\alpha$  revealed significant positive correlation to BUN and s. creatinine levels. Inflammation was reported to play a crucial role in tissue damage after ischemia reperfusion. Chemokines and cytokines overproduction in addition to activation of complement system enhance the proinflammatory leukocytic infiltration into post-ischemic regions of the kidneys that may occur within few hours of tissue injury [42]. Different studies have shown that renal dendritic cells infiltration and several chemokines in particular, IL-1b, IL-6, TGF- $\beta$  and  $\text{TNF}\alpha$  are capable of damaging endothelial cells and increasing vascular permeability, with a subsequent reduction in renal blood flow in the IR kidneys [43-44].

In addition, renal tissue nitrate level was significantly decreased in IRI group which may provide another explanation for the reduced oxidant defense mechanisms in this group, as nitrate was proved to have anti-oxidant effects [52].

Moreover, deficient antiapoptotic responses might explain the severe deleterious functional and structural effects appeared on kidneys of IR group of rats. In our study, week positive BCL2 anti-apoptotic reaction in immune-histochemical study of this group was observed. In parallel, apoptosis was previously reported by Kunduzova et al (2003) [53] in renal tubular cells after IR in an *in-vivo* and *in-vitro* model of renal injury and attributed these findings to caspase-3 activation, which represents a direct mechanism for tubular damage.

In the kidney, sympathetic nerve fibers are closely related to inflammatory cells and immunocytes such as macrophages and dendritic cells [54]. Sympathetic nerve fibers are involved in neuro-immune interplay in the kidney via increased cytokine-stimulated sympathetic nerve activity [54-56] and through production of Ang II which is widely known as a hypertensive and pro-inflammatory mediator [57]. Therefore, RDN could improve the renal functions, structure and ultra-structure.

Interestingly enough, the increase of renal function values was partially corrected by RDN (as demonstrated by the significant reduction of BUN compared to IR group) while the values of BUN and serum creatinine [26] were nearly normalized in RDN-VNS group. Improvement of renal functions indicated regression of the stage of kidney from ARF to AKI. The amelioration of inflammatory, oxidative and anti-apoptotic markers could explain such improvement. We had supported these results by histological study (light and electron microscopic examinations). The oxidant / anti-oxidant imbalance observed in the IR group was improved in the group which was underwent RDN.

Meanwhile, the combination of RDN and VNS reduced the oxidative stress dependent tissue damage, and restored the antioxidant defense mechanism as serum MDA was significantly decreased and the renal tissue GPX anti-oxidant enzyme activity was significantly increased to the normal levels in RDN-VNS

group becoming comparable to the sham group. In addition, renal tissue nitrate level was significantly increased in the RDN group and further elevated in the RDN-VNS group to the normal level. Therefore, VNS conferred more protective effect when combined to RDN.

Consistently, RDN was reported to be protective against renal failure by different mechanisms such as decreasing blood pressure and down-regulation of the renin-angiotensin system [58,59].

We had supported the functional ameliorative effects of RDN on IR induced kidney damage and the reno-protective effects of combining RDN to VNS by the histological examination. The H and E study of the renal cortex of RDN kidneys showed that some of the renal corpuscles, glomeruli and Bowman's spaces were average in size and shape but others showed slightly congested glomeruli and little widening of Bowman's space. On the other hand, the majority of the glomeruli of RDN-VNS group were to some extent as those of the sham group and higher magnification showed that most of the renal corpuscles of the RDN-VNS rats were intact as the glomeruli were normal and Bowman's capsules were patent. Also, some tubules of RDN group seemed free from exfoliation in their luminae but others contained exfoliation and intracellular cytoplasmic vacuoles while, proximal, distal and collecting tubules were normally shaped in RDN-VNS group. In addition, the mononuclear cellular infiltration in the interstitial tissues around the injured areas in IR group was also declined in RDN group and markedly decreased in RDN-VNS group. The renal cortex showed few collagen fibers around the renal capsules, the glomeruli and the tubules of RDN rats and minimal collagen fibers around the Bowman's capsules and the tubules of RDN-VNS rats. Also, septa between tubules were intact in comparison to IR group in both RDN groups.

EM study of RDN kidneys showed that the podocytes had partial disorganized pedicles and electron-dense substances in the glomerular capillaries. Whereas, the podocytes of RDN-VNS group showed euchromatic indented nuclei and mitochondria with normal arranged secondary feet processes. Also, in RDN-VNS group, the space between the pedicles (filtration slits) could be seen and laid on a regular glomerular basement membrane. Though, some of the podocytes showed distorted and fused feet processes with the appearance of few matrixes around mesangial cells in both RDN groups. Lumens of the PCT of RDN group were filled with secretions and the lining cells of the tubules showed microvilli, small cytoplasmic vacuoles and small dense lysosomes but some of their mitochondria were swollen. On the other hand, the cells of the PCT in RDN-VNS, revealed normally appeared long, dense apical microvilli and basal enfolding in addition to presence of few and small pinocytic vesicles near to the lysosomes. The cells of the DCT of RDN group revealed small lysosomes and areas of cytoplasmic rarefaction could be observed. Some nuclei were irregular in shape and shrunken, but others were nearly average in appearance. While, most of the nuclei were normal in appearance, but scanty of them were pyknotic in DCT of RDN-VNS group.

Also, the inflammatory marker TNF $\alpha$  level in renal tissue was decreased in the RDN and further decreased in the RDN-VNS groups compared to the IR group. Additionally, the NO metabolite (nitrate) was significantly increased in renal tissue, which has also an anti-inflammatory effect in the RDN-VNS group. The aforementioned changes observed in RDN-VNS group led to prevention of renal damage following IRI as the renal function tests (BUN& Serum creatinine) were positively correlated to the inflammatory marker, TNF $\alpha$ .

In agreement to our findings, inflammation was reduced markedly in RDN kidneys as renal expression of TNF $\alpha$  and macrophages accumulation were reduced [60]. Fibrosis was also diminished as indicated by reduced TGF- $\beta$  expression and glomerular collagen IV deposition in RDN rats [61]. Consistently, the associated IR induced renal tissue damage was reported to be attenuated by both surgical and drug induced blockade of renal sympathetic nerve activity [8]. In deed renal sympathetic nerve stimulation is a primary mechanism instigating fibrogenesis in the IR induced AKI [12]. Additionally, it was also found that RDN prevented unilateral ureteral obstruction-induced inflammation and interstitial fibrosis [62]. Moreover, RDN prior to or up to 1 day post-ischemic renal injury attenuated the associated tubular injury, apoptosis, tubulointerstitial inflammation and fibrosis and preserved kidney function during the early post-ischemic period [12]. Furthermore, centrally acting sympatholytics (i.e. clonidine and moxonidine) have been shown to prevent IR induced AKI [63].

Our results revealed that efferent VNS in combination with RDN further protected against IRI, preserved renal function and structure and suppressed TNF- $\alpha$  induction when performed 10 min before renal ischemia. Parallel to our findings, other investigators deduced that electrical stimulation of the efferent VN significantly decreased the amounts of TNF $\alpha$  in the serum [60]. In former literature done by INOUE et al. [8], afferent or efferent VNS was performed 24 hours before ischemia to obtain the renoprotective effects while, immediate responses to VNS (10 min before ischemia) were unsuccessful.

VNS, via vago-sympathetic reflexes, was assumed to have two opposing effects on kidney in IRI; an anti-inflammatory effect through activation of sympathetic splenic nerve, the so called cholinergic anti-inflammatory pathway (CAP) and a pro-inflammatory deleterious effect through stimulation of renal sympathetic nerves. Cholinergic anti-inflammatory pathway (CAP) is a neuro-immune pathway which inhibits inflammation through the suppression of cytokine production and prevents damage [65-67]. The parasympathetic innervation of the spleen remains controversial because some studies have shown a direct innervation of the spleen by the VN [68] whereas others denied this connection [69]. In addition, choline acetyltransferase, a more specific marker of cholinergic nerve fibers than acetylcholine-esterase, is absent in the spleen [70]. CAP is spleen-dependant and VNS-induced inhibition of systemic TNF- $\alpha$  production was abolished in splenectomized animals [71]. These data argue for a link between the spleen and the CAP via the VN through the splenic sympathetic nerve [64]. Further support comes from studies demonstrating that stimulation of the

splenic CAP with ultrasounds ameliorates IR induced AKI in mice [72-73].

Stimulation of the CAP by VNS inhibits cytokine synthesis through ACh which decreases the production of pro-inflammatory cytokines such as TNF $\alpha$  by binding to ACh receptors expressed by cytokine-producing cells and macrophages [64]. The  $\alpha 7$  subunit of the nicotinic AChR ( $\alpha 7$ nAChR) is the best recognized of these cholinergic receptors that suppress cytokines [64, 74]. Therefore, ACh released by the VN in the celiac-mesenteric ganglia activates postsynaptic  $\alpha 7$ nAChR of the splenic sympathetic nerve, leading to the release of NE in the spleen thus inhibiting the production and secretion of TNF $\alpha$  by splenic macrophages [75]. Muscarinic as well as nicotinic receptors are also found on T lymphocytes [67].

However, VNS when done 10 minutes prior to ischemia, it offered no protection in earlier advances. Renal protection and suppression of TNF- $\alpha$  induced by CAP via vago-sympathetic reflex was long lasting and at least, 24 h should elapse after VNS to show its protective role before renal ischemia [8,72,73].

On the other hand, stimulation of renal sympathetic nerves by vago-sympathetic reflex may have contradictory effect to the anti-inflammatory effects of VNS in AKI which gives an appreciable explanation for the long duration needed for VNS to perform its reno-protection. The stimulation of renal sympathetic nerve and increased renal norepinephrine levels play important roles in pathogenesis and development of renal IR induced injury and administration of recombinant renalase ameliorated renal function and histological kidney damage by suppressing overproduction of norepinephrine levels [77]. It was also reported that yohimbine, and  $\alpha 2$ -adrenoceptor antagonist, protects against renal IRI in rats [78]. Therefore, in our study, the accelerated response to VNS might be accounted for by surgical sympathetic ablation by RDN. Results of our study didn't show only an anti-inflammatory effect to VNS in the RDN-VNS group, but anti-oxidant and anti-apoptotic effects as well. Immuno-histochemical study of Bcl2 exhibited moderately positive immune-reaction in kidneys of RDN group and strong positive one in RDN-VNS group indicating strong anti-apoptotic effect of RDN which became more apparent after VNS. Interestingly, Bcl2 were needed for regenerating proximal tubules after an ischemic injury [79, 80].

Therefore restoration of oxidant/antioxidant balance in addition to apoptotic and anti-inflammatory effects are important strategies of VNS for protecting the renal tissue from IR injury.

## Conclusion

RDN could alone protect against IRI, at least partially. Synergism between RDN and VNS enhanced and accelerated the reno-protection via restoration of oxidant/antioxidant balance, anti-inflammatory and anti-apoptotic effects. Taken together, RDN and VNS in combination conferred an optimized functional, structural and ultra-structural renal protection in IR induced AKI.

## Competing Interests

The authors declare no competing or financial interests.

## Acknowledgment

We would like to thank and acknowledge Faculty of Medicine, Ain Shams University for partial funding of the work, Dr. Shadwa Khaled., Dr. Farah Shafeeq, Dr. Abdalla Magdy., Dr. Mohamed Mahmoud Ismaiel, and Dr. Mohamed Fahmy for their hard and kind support during the practical work of the study.

Ethical approval: All experimental procedures were approved from the ethics committee in Ain Shams Faculty of Medicine.

Data Availability statements: All included and individual data are available upon request.

Funding statement: This work is partially funded by faculty of medicine, Ain Shams University

## References

1. Coca SG, Singanamala S, Parikh CR (2012) Chronic kidney disease after acute kidney injury: A systematic review and meta-analysis. *Kidney Int* 81: 442-448.
2. Schiffli H, Lang SM, Fischer R (2012) Long-term outcomes of survivors of ICU acute kidney injury requiring renal replacement therapy: A 10-year prospective cohort study. *Clin Kidney J* 5: 297-302.
3. Rifkin DE, Coca SG, Kalantar-Zadeh K (2012) Does AKI truly lead to CKD? *J Am Soc Nephrol* 23: 979-984.
4. Kellum JA, Unruh ML, Murugan R (2011) Acute kidney injury. *BMJ Clin Evid*.
5. Hoste EAJ, Clermont G, Kersten A, Venkataraman R, Angus DC, et al. (2006) RIFLE criteria for acute kidney injury are associated with hospital mortality in critically ill patients: a cohort analysis. *Crit Care* 10: R73.
6. Zimmerman BJ, Granger DN (1992) Reperfusion injury. *Surg Clin North Am* 72: 65-83.
7. Lien YH, Lai L, Silva AL (2003) Pathogenesis of renal ischemia/reperfusion injury: lessons from knockout mice. *Life Sci* 74: 543-552.
8. Inoue T, Abe C, Sung SS, Moscalu S, Jankowski J, et al. (2016) Vagus nerve stimulation mediates protection from kidney ischemia-reperfusion injury through  $\alpha 7$ nAChR+ splenocytes. *Clin Invest* 126: 1939-1952.
9. Gallowitsch-Puerta M, Pavlov VA (2007) Neuro-immune interactions via the cholinergic anti-inflammatory pathway. *Life Sci* 80: 2325-2329.
10. Iaina A, Eliahou HE (1983) The sympathetic nervous system in the pathogenesis of acute renal failure. *Clin Exp Dial Apheresis* 7: 115-125.
11. Schlaich MP, Socratous F, Hennebry S, Eikelis N, Lambert EA, et al. (2009) Sympathetic activation in chronic renal failure. *J Am Soc Nephrol* 20: 933-939.
12. Kim J, Padanilam BJ (2015) Renal denervation prevents long-term sequelae of ischemic renal injury. *Kidney Int* 87: 350-358.

13. Borovikova LV, Ivanova S, Zhang M, Yang H, Botchkina GI, et al. (2000) Vagus nerve stimulation attenuates the systemic inflammatory response to endotoxin. *Nature* 405: 458-462.
14. Stacey WC, Litt B (2008) Technology insight: neuroengineering and epilepsy-designing devices for seizure control. *Nat Clin Pract Neurol* 4: 190-201.
15. Rosas-Ballina M, Olofsson PS, Ochani M, Valdés-Ferrer SI, Levine YA, et al. (2011) Acetylcholine-synthesizing T cells relay neural signals in a vagus nerve circuit. *Science* 334: 98-101.
16. Levine YA, Koopman FA, Faltys M, Caravaca A, Bendele A, et al. (2014) Neurostimulation of the cholinergic anti-inflammatory pathway ameliorates disease in rat collagen-induced arthritis. *PLoS One* 9.
17. Zhang YL, Zhang J, Cui LY, Yang S (2015) Autophagy activation attenuates renal ischemia-reperfusion injury in rats. *Exp Biol Med* 240: 1590-1598.
18. Patton CJ, Crouch SR (1997) Spectrophotometric and kinetics investigation of the Berthelot reaction for the determination of ammonia. *Anal Chem* 49: 464-469.
19. Bartels H, Bohmer M, Heierli C (1972) Serum creatinine determination without protein precipitation. *Clin Chem Acta* 37: 193-197.
20. Draper HH, Hadley M (1991) Malondialdehyde determination as index of lipid peroxidation. *Methods Enzymol* 186: 421-443.
21. Paglia DE, Valentine WN (1967) Studies on the quantitative and qualitative characterization of erythrocyte glutathione peroxidase. *J Lab Clin Med* 70: 158-169.
22. Marín-García J, Goldenthal MJ, Moe GW (2001) Abnormal cardiac and skeletal muscle mitochondrial function in pacing-induced cardiac failure. *Cardiovasc Res* 52: 103-110.
23. Bories PN, Bories C (1995) Nitrate determination in biological fluids by an enzymatic one step assay with nitrate reductase. *Clin Chem* 41: 904-907.
24. Suvarna K, Layton C, Bancroft J (2013) Bancroft's theory and practice of histological techniques. 8th edition. Churchill Livingstone: Philadelphia 173-212.
25. Waikar SS, Bonventre JV (2007) Biomarkers for the diagnosis of acute kidney injury. *Curr Opin Nephrol Hypertens* 16: 557-564.
26. Barasch J, Zager R, Bonventre JV (2017). Acute kidney injury: a problem of definition. *Lancet* 389: 779-781.
27. Mehta RL, Burdmann EA, Cerdá J, Feehally J, Finkelstein F, et al. (2016) Recognition and management of acute kidney injury in the International Society of Nephrology Oby25 Global Snapshot: a multinational cross-sectional study. *Lancet* 387: 2017-2025.
28. Gao Y, Chen L, Ning Y, Cui X, Yin L, et al. (2014) Chen J, Wang J, Shao B, Xu D: Hydro-Jet-assisted laparoscopic partial nephrectomy with no renal arterial clamping: A preliminary study in a single center. *Int Urol Nephrol* 46: 1289-1293.
29. Aziz JS (2015) The structural and functional changes induced by lithium on the renal cortex of Growing albino Rats: Ultrastructure and laboratory study. *Acta Medica International* 2: 70-78.
30. Forbes JM, Hewitson TD, Becker GJ, Jones CL (2000) Ischemic acute renal failure: Long-term histology of cell and matrix changes in the rat. *Kidney Int* 57: 2375-2385.
31. Ahmed SM, Mahmoud AA, Hassen EZ, Abdel Kader RR (2018) Light and electron microscope study on the effect of platelet-rich plasma in induced renal ischaemia-reperfusion injury in the renal cortex of adult male albino rats. *J Biochem Cell Biol* 1: 1-8.
32. Hotchkiss RS, Strasser A, McDunn JE, Swanson PE (2009) Cell death. *N Engl J Med* 361: 1570-1583.
33. Chen X, Sun C, Chen Q, O'Neill FA, Walsh D, et al. (2009) Apoptotic engulfment pathway and schizophrenia. *PLoS One* 4: e6875.
34. Elliott MR, Chekeni FB, Trampont PC, Lazarowski ER, Kadl A, et al. (2009) Nucleotides released by apoptotic cells act as a find-me signal to promote phagocytic clearance. *Nature* 461: 282-286.
35. Kacmaz A, Polat A, User Y, Tilki M, Ozkan S, et al. (2004) Octreotide improves reperfusion-induced oxidative injury in acute abdominal hypertension in rats. *J Gastrointest Surg* 8: 113-119.
36. Johnson KJ, Weinberg JM (1993) Postischemic renal injury due to oxygen radicals. *Curr Opin Nephrol Hypertens* 2: 625-635.
37. Paller MS (1994) The cell biology of reperfusion injury in the kidney. *J Investig Med* 42: 632-639.
38. Bonventre JV (1993) Mechanisms of ischemic acute renal failure. *Kidney Int* 43: 1160-1178.
39. Peng TI, Jou MJ (2010) Oxidative stress caused by mitochondrial calcium overload. *Ann N Y Acad Sci* 1201: 183-188.
40. Kalogeris T, Baines CP, Krenz M, Korthuis RJ (2012) Cell biology of ischemia/reperfusion injury. *Int Rev Cell Mol Biol* 298: 229-317.
41. Singh I, Gulati S, Orak JK, Singh AK (1993) Expression of antioxidant enzymes in rat kidney during ischemia-reperfusion injury. *Mol Cell Biochem* 125: 97-104.
42. Jang HR, Rabb H (2015) Immune cells in experimental acute kidney injury. *Nat Rev Nephrol* 11: 88-101.
43. Singh V, Jain S, Gowthaman U, Parihar P, Gupta P, et al. (2011) Co-administration of IL-1 + IL-6 + TNF-alpha with Mycobacterium tuberculosis infected macrophages vaccine induces better protective T cell memory than BCG. *PLoS One* 6: e16097.
44. Schreiber S, Nikolaus S, Hampe J, Hämling J, Koop I, et al. (1999) Tumour necrosis factor alpha and interleukin 1beta in relapse of Crohn's disease. *Lancet* 353: 459-461.
45. Kanner J, Harel S, Granit R (1991) Nitric oxide as an antioxidant. *Arch Biochem Biophys* 289: 130-136.
46. Granger DN, Kubes P (1996) Nitric oxide as antiinflammatory agent. *Methods Enzymol* 269: 434-442.
47. Phillips L, Toledo AH, Lopez-Neblina F, Anaya-Prado R, Toledo-Pereyra LH (2009) Nitric oxide mechanism of protection in ischemia and reperfusion injury. *J Invest Surg* 22: 46-55.
48. Duranski MR, Greer JJ, Dejam A, Jaganmohan S, Hogg N, et al. (2005) Cytoprotective effects of nitrite during in vivo ischemia-reperfusion of the heart and liver. *J Clin Invest* 115: 1232-1240.
49. Jung KH, Chu K, Ko SY, Lee ST, Sinn DI, et al. (2006) Early intravenous infusion of sodium nitrite protects brain against in vivo ischemia-reperfusion injury. *Stroke* 37: 2744-2750.
50. Lu P, Liu F, Yao Z, Wang CY, Chen DD, et al. (2005) Nitrite-derived nitric oxide by xanthine oxidoreductase protects the liver against ischemia-reperfusion injury. *Hepatobiliary Pancreat Dis Int* 4: 350-355.
51. Tripatara P, Patel NS, Webb A, Rathod K, Lecomte FM, et al. (2007) Nitrite-derived nitric oxide protects the rat kidney against ischemia/reperfusion injury in vivo: role for xanthine oxidoreductase. *J Am Soc Nephrol* 18: 570-580.

52. Hammad FT, Al-Salam S, Lubbad L (2013) Does aliskiren protect the kidney following ischemia reperfusion injury? *Physiol Res* 62: 681-690.
53. Kunduzova OR, Escourrou G, Seguelas MH, Delagrangre P, De La Farge F, et al. (2003) Prevention of apoptotic and necrotic cell death, caspase-3 activation, and renal dysfunction by melatonin after ischemia/reperfusion. *FASEB J* 17: 872-874.
54. Kaissling B, Le Hir M (1994) Characterization and distribution of interstitial cell types in the renal cortex of rats. *Kidney Int* 54: 709-720.
55. Soos TJ, Sims TN, Barisoni L, Lin K (2006) Littman DR, Dustin ML, Nelson PJ: CX3CR+ interstitial dendritic cells form a contiguous network throughout the entire kidney. *Kidney Int* 70: 591-596.
56. Zhang ZH, Wei SG, Francis J, Felder RB (2003) Cardiovascular and renal sympathetic activation by blood-borne TNF $\alpha$  in rat: The role of central prostaglandins. *Am J Physiol Regul Integr Comp Physiol* 284: R916-R927.
57. Phillips MI, Kagiya S (2002) Ang II as a pro-inflammatory mediator. *Curr Opin Investig Drugs* 3: 569-577.
58. DiBona GF (2005) Physiology in perspective: The wisdom of the body. Neural control of the kidney. *Am J Physiol Regul Integr Comp Physiol* 289: R633-641.
59. Clayton SC, Haack KKV, Zucker IH (2011) Renal denervation modulates angiotensin receptor expression in the renal cortex of rabbits with chronic heart failure. *Am J Physiol Renal Physiol* 300: F31-F39.
60. Veelken R, Vogel EM, Hilgers K, Amann K, Hartner A, et al. (2008) Autonomic renal denervation ameliorates experimental glomerulonephritis. *J Am Soc Nephrol* 19: 1371-1378.
61. Fujii T, Kurata H, Takaoka M, Muraoka T, Fujisawa Y, et al. (2003) The role of renal sympathetic nervous system in the pathogenesis of ischemic acute renal failure. *Eur J Pharmacol* 481: 241-248.
62. Kim J, Padanilam BJ (2013) Renal nerves drive interstitial fibrogenesis in obstructive nephropathy. *J Am Soc Nephrol* 24: 229-242.
63. Tsutsui H, Sugiura T, Hayashi K, Ohkita M, Takaoka M, et al. (2009). *Eur J Pharmacol* 603: 73-78.
64. Bonaz B, Picq C, Sinniger V, Mayol JF, Clarencon D (2013) Vagus nerve stimulation: from epilepsy to the cholinergic anti-inflammatory pathway. *Neurogastroenterol Motil* 25: 208-221.
65. Tracey KJ (2007) Physiology and immunology of the cholinergic anti-inflammatory pathway. *J Clin Invest* 117: 289-296.
66. Olofsson PS, Rosas-Ballina M, Levine YA, Tracey KJ (2012) Rethinking inflammation: neural circuits in the regulation of immunity. *Immunol Rev* 248: 188-204.
67. Pavlov VA, Tracey KJ (2012) The vagus nerve and the inflammatory reflex-linking immunity and metabolism. *Nat Rev Endocrinol* 8: 743-754.
68. Buijs RM, van der Vliet J, Garidou ML, Huitinga I, Escobar C (2008) Spleen vagal denervation inhibits the production of antibodies to circulating antigens. *PLoS One* 3: e3152.
69. Bratton BO, Martelli D, McKinley MJ, Trevaks D, Anderson CR, et al. (2012) Neural regulation of inflammation: no neural connection from the vagus to splenic sympathetic neurons. *Exp Physiol* 97: 1180-1185.
70. Bellinger DL, Lorton MD, Hamill RW, Felten SY, Felten DL (1993) Acetylcholinesterase staining and choline acetyltransferase activity in the young adult rat spleen: lack of evidence for cholinergic innervation. *Brain Behav Immun* 7: 191-204.
71. Huston JM, Ochani M, Rosas-Ballina M, Liao H, Ochani K, et al. (2006) Splenectomy inactivates the cholinergic anti-inflammatory pathway during lethal endotoxemia and polymicrobial sepsis. *J Exp Med* 203: 1623-1628.
72. Gigliotti JC, Huang L, Ye H, Bajwa A, Chattrabuthi K, et al. (2013) Ultrasound prevents renal ischemia-reperfusion injury by stimulating the splenic cholinergic anti-inflammatory pathway. *J Am Soc Nephrol* 24: 1451-1460.
73. Gigliotti JC, Huang L, Bajwa A, Ye H, Mace EH, et al. (2015) Ultrasound modulates the splenic neuroimmune axis in attenuating AKI. *J Am Soc Nephrol* 26: 2470-2481.
74. Pavlov VA, Wang H, Czura CJ, Friedman SG, Tracey KJ (2003) The cholinergic anti-inflammatory pathway: A missing link in neuroimmunomodulation. *Mol Med* 9: 125-134.
75. Rosas-Ballina M, Ochani M, Parrish WR, Ochani K, Harris YT, et al. (2008) Splenic nerve is required for cholinergic anti-inflammatory pathway control of TNF in endotoxemia. *Proc Natl Acad Sci* 105: 11008-11013.
76. Nizri E, Hamra-Amitay Y, Sicsic C, Lavon I, Brenner T (2006) Anti-inflammatory properties of cholinergic up-regulation: a new role for acetylcholinesterase inhibitors. *Neuropharmacology* 50: 540-547.
77. Lee HT, Kim JY, Kim M, Wang P, Tang L, et al. (2013) Renalase protects against ischemic AKI. *J Am Soc Nephrol* 24: 445-455.
78. Shimokawa T, Tsutsui H, Miura T, Nishinaka T, Terada T, et al. (2016) Renoprotective effect of yohimbine on ischaemia/reperfusion-induced acute kidney injury through  $\alpha$ 2C-adrenoceptors in rats. *Eur J Pharmacol* 781: 36-44.
79. Basile DP, Liapis H, Hammerman MR (1997) Expression of bcl-2 and bax in regenerating rat renal tubules following ischemic injury. *Am J Physiol* 272: F640-F647.
80. Ajami M, Davoodi SH, Habibey R, Namazi N, Soleimani M, et al. (2013) Effect of DHA+EPA on oxidative stress and apoptosis induced by ischemia-reperfusion in rat kidneys. *Fundam Clin Pharmacol* 27: 593-602.